DETERMINATION OF LIFETIMES OF EXCITED STATES IN NEUTRON-RICH ^{20}O ISOTOPE FROM EXPERIMENT WITH THE AGATA+PARIS+VAMOS SETUP*

M. Ciemała[a], S. Ziliani[b,c], F. Crespi[b,c], S. Leoni[b,c], B. Fornal[a]
A. Maj[a], P. Bednarczyk[a], G. Benzoni[c], A. Bracco[b,c], C. Boiano[c]
S. Bottoni[b,c], S. Brambilla[b], M. Bast[d], M. Beckers[d]
T. Braunroth[d], F. Camera[b,c], N. Cieplicka-Oryńczak[a]
E. Clément[e], O. Dorvaux[f], S. Ertürk[g], G. De France[e]
A. Goldkuhle[d], J. Grębosz[a], M.N. Harakeh[h], Ł.W. Iskra[a]
B. Jacquot[e], A. Karpov[i], M. Kicińska-Habior[j], Y. Kim[e]
M. Kmiecik[a], A. Lemasson[e], H. Li[e], I. Matea[k], K. Mazurek[a]
C. Michelagnoli[l], B. Millon[c], C. Müller-Gatermann[d]
P. Napiorkowski[m], V. Nanal[n], M. Matejska-Minda[m]
M. Rejmund[e], B. Sowicki[a], Ch. Schmitt[f], M. Stanoiu[o], I. Stefan[k]
B. Wasilewska[a], M. Zielińska[p], M. Ziębliński[a]

[a]Institute of Nuclear Physics Polish Academy of Sciences, 31-342 Kraków, Poland
[b]Università degli Studi di Milano, Via Celoria 16, 20133, Italy
[c]INFN, sezione di Milano, Italy
[d]IKP Cologne, Cologne, Germany
[e]GANIL, CEA/DSAM and CNRS/IN2P3, CAEN Cedex 05, France
[f]CNRS/IN2P3, IPHC UMR 7178, F-67037 Strasbourg, France
[g]Nigde University, Turkey
[h]KVI — Center for Advanced Radiation Technology, Groningen, The Netherlands
[i]JINR, Dubna, Russia
[j]Faculty of Physics, Warsaw University, Warszawa, Poland
[k]IPN Orsay Laboratory, Orsay, France
[l]Institut Laue-Langevin (ILL), Grenoble, France
[m]Heavy Ion Laboratory, University of Warsaw
Pasteura 5A, 02-093 Warszawa, Poland
[n]Department of Nuclear and Atomic Physics
Tata Institute of Fundamental Research, Mumbai 400005, India
[o]IFIN-HH, Bucharest, Romania
[p]IRFU, CEA/DRF, Centre CEA de Saclay, 91191 Gif-sur-Yvette Cedex, France

---

An experiment aiming at measuring lifetimes of the second 2^+ excited states in neutron-rich C and O isotopes was recently performed at the GANIL laboratory, in France. In these nuclei, recent *ab initio* calculations provide a detailed description of the nuclear excited states, predicting a strong sensitivity of the electromagnetic transition probabilities to the details of the nucleon–nucleon interactions, especially in connection with the role played by the three-body (NNN) forces. Thus, the measurement of 2^+ states lifetimes in this region will be a stringent test of the importance of including the NNN forces in describing the electromagnetic properties of selected nuclear states. This contribution reports on the status of the experimental analysis for the case of lifetimes in ^{20}O.

1. Introduction

Aim of the measurement was to determine the lifetimes (in the range of hundreds of femtoseconds) of the excited states in neutron-rich C and O isotopes, in particular in ^{16}C and ^{20}O. For these nuclei, *ab initio* calculations predict a strong sensitivity of selected electromagnetic transition probabilities to the details of the nucleon–nucleon interactions, especially to the three-body term. Strong sensitivity is expected, in particular, in the case of the second excited 2^+ state, in each nucleus of interest. For example, the calculated value of the 2_2^+ state lifetime in O^{20} is equal to 320 fs (with NN interactions), compared to 200 fs, obtained including NN + NNN interactions [1, 2].

The experiment was performed in the GANIL laboratory, with a combined detector setup including the segmented HPGe detectors of the AGATA tracking array [3, 4], the VAMOS spectrometer [5] and the PARIS scintillator-based calorimeter [6]. In order to cover the lifetime range of interest (below 500 fs), the technique involving the γ-ray lineshape analysis (DSAM — Doppler-Shift Attenuation Method) was used.

2. Experimental details

The nuclei of interest were populated in the deep inelastic processes induced by an ^{18}O beam at 126 MeV (7.0 MeV/u) on a ^{181}Ta target, 6.64 mg/cm^2 thick (4 μm). The beam energy at the center of the target was ~ 116 MeV, *i.e.* 50% above the Coulomb barrier, and the projectile-like products had $v/c \sim 10\%$. The experimental setup contained 31 AGATA crystals placed at backward angles with respect to the entrance of the VAMOS spectrometer (from $\sim 120°$ to $\sim 175°$) and two PARIS clusters (one with LaBr$_3$:NaI- and the second with CeBr:NaI-type phoswiches) with two additional large volume LaBr$_3$ detectors at $\sim 90°$ (Fig. 1).
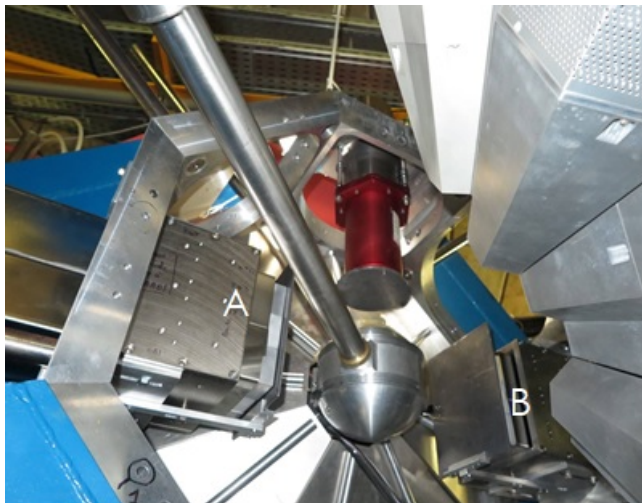
Fig. 1. Photograph of the experimental setup. The letters A and B mark the PARIS clusters containing LaBr$_3$:NaI and CeBr:NaI phoswiches, respectively. Above (and below) the reaction chamber, there are placed two large volume (3.5″ × 8″) LaBr$_3$ detectors. On the right-hand side photo, there are visible the AGATA modules.

The VAMOS spectrometer was placed at the maximum (45°) angle with respect to the beam axis. Its focal plane contains:

— four drift chambers, which give information on x_f, y_f position for the reconstruction of the θ_f, ϕ_f angles;

— segmented (six columns, four rows) ionization chambers measuring the ion energy loss ΔE;

— plastic scintillator at the end of the focal plane, which gives: trigger signal, particle energy E and time with respect to the radio frequency (RF).

Moreover, two additional pairs of drift chambers were put at the entrance of VAMOS (20 cm from the target) for a better determination of the ions entrance θ, ϕ, which was done to improve the γ-ray Doppler correction [7]. The γ decay of the identified reaction products was measured with the AGATA array and the PARIS detectors. Using the velocity vector $\vec{v}$ reconstructed in VAMOS, a Doppler correction was applied to the γ-ray spectra. Calibration and fine tuning of the AGATA detectors is presented in [8].

3. Data analysis

In order to apply the DSAM method in the present experiment, it is very important to precisely determine $\vec{v}$ of the ions which emitted γ rays. For this purpose, all of the VAMOS focal plane detectors were calibrated and tuned. These are the main adjustments that have been performed:

— gain matching for the drift chamber wires;

— energy calibration of the ionization chambers and check of their stability during the time of the experiment;

— time and energy calibration of the plastic detector.

Then, one can obtain ions velocity v by

$$v = D/T\,,$$

where D is the ion path length from the target to the plastic detector and T is the time of flight calculated as a difference between the RF signal of the cyclotron and the plastic detector time-signals (time between following beam pulses was equal to 102 ns).

To be sure that the ions time-of-flight value is correct, one has to check if the masses obtained using this time are reconstructed in the proper way. Unfortunately, the masses are calculated using $(M/Q) \times Q$, which is correlated to both time and energy. Therefore, one has to simultaneously check time and energy calibrations. Firstly, (M/Q) is calculated

$$M/Q = \frac{B\rho}{3.105\gamma\beta}\,,$$

where $B\rho$ is reconstructed using the dedicated library (libVAMOS) from the θ_f, ϕ_f values, $B\rho_\mathrm{ref}$ (which was equal to 0.75 Tm for this experiment) and the VAMOS response function.

Then

$$
\begin{aligned}
M_0 &= \frac{E_\mathrm{tot}}{931.5016(\gamma - 1)}\,, \\
Q &= M_0/(M/Q)\,,
\end{aligned}
$$

where E_tot is total energy (sum of ΔE measured by ionization chambers and E from plastic detector) and M_0 is mass extracted from total energy.

Finally, the reconstructed mass M_r is

$$M_\mathrm{r} = M/Q \times Q_\mathrm{int}\,,$$

where Q_int is the nearest integer value of Q.

To choose ion's atomic number Z, one has to select the corresponding region in the ΔE–E_{tot} matrix (Fig. 2, with gate on the $Z = 8$ region). Using the technique described above, the plot of Q *versus* M_{r} can be obtained. Such a plot for $Z = 8$ is shown in Fig. 3 — here, two oxygen ions charge states are visible, with $Q = 8$ and 7.

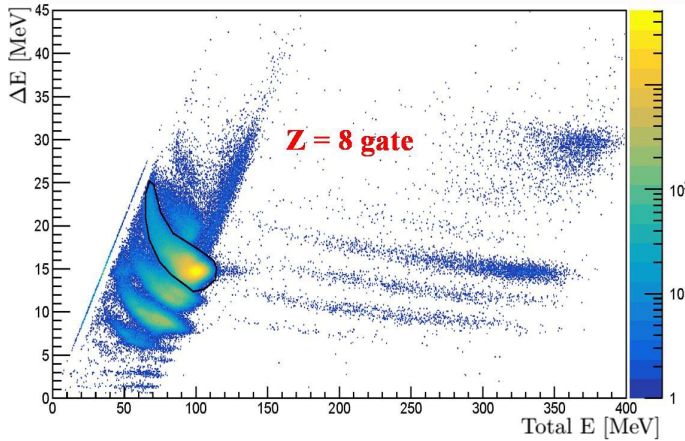Fig. 2. ΔE–E_{tot} plot with region corresponding to $Z = 8$ selection (part of data).
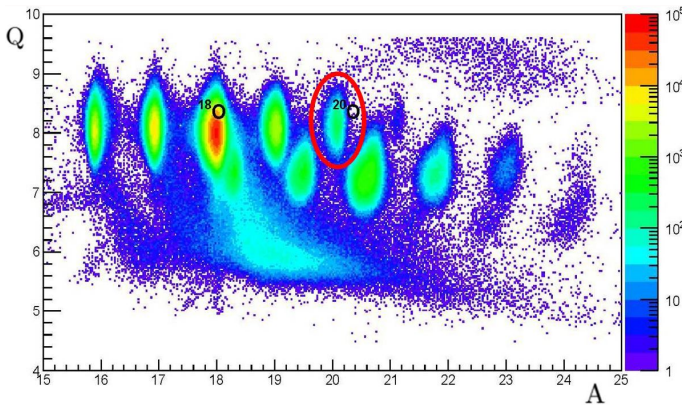

Fig. 3. Plot of ions' charge Q *versus* their mass A reconstructed using the VAMOS focal plane detectors (part of data). (For better readability, the formula $M_{\text{r}} = M/Q \times 8$ was used, so masses for $Q = 7$ are shifted.)

By checking product intensity as a function of mass for $Z = 5$ to 9, very good agreement with the expected mass distribution was observed: this means that the time and energy calibration of the VAMOS focal plane are done properly. Figure 4 shows the populations intensity of the ions identified in this experiment.
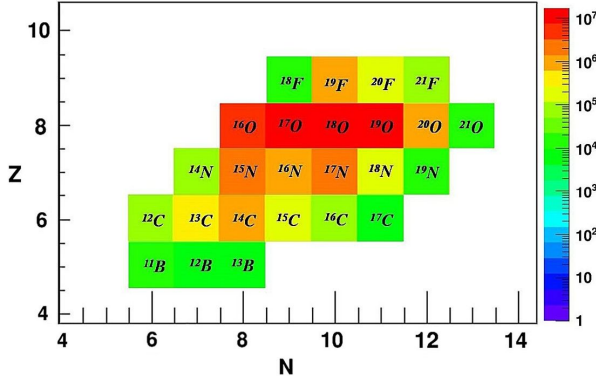
Fig. 4. Graph presenting the population of detected and identified ions during the experiment.

Check of the stability of the reconstructed masses values (M_r) in the course of measurement was also performed. The upper panel of Fig. 5 shows the evolution of the reconstructed ^{18}O ion mass with respect to the time of the experiment. A drift is visible with the same pattern as drift of the PARIS time-signal with respect to RF (middle panel of Fig. 5). In consequence, by applying a correction to the ion T extracted from PARIS time $vs.$ RF, one can obtain a better stability of the reconstructed masses (bottom panel of Fig. 5).

For PARIS detectors, the energy calibration was done with the use of standard ^{60}Co, ^{137}Cs, ^{152}Eu γ-ray sources as well as AmBe–Fe for calibration points in the high-energy region (up to 7 MeV). Gating on the ^{20}O ions and the proper PARIS time with respect to RF signal, the Doppler-corrected spectrum in Fig. 6 was obtained, with $2_2^+ \rightarrow 2_1^+$ (line of interest) and $4^+ \rightarrow$ g.s. transitions visible. PARIS data will be used for measuring the γ-ray angular distributions, providing a reference point for the angle around $90°$.

Finally, in Fig. 7, the Doppler-corrected AGATA γ-ray spectrum gated on ^{20}O is presented: the transition of interest, $2_2^+ \rightarrow 2_1^+$ 2396 keV, is clearly displayed. The potential of the present measurement in accessing the lifetime of the transition of interest is shown in Fig. 8. Here, the relative differences between the measured and the tabulated γ-ray energy for $2_1^+ \rightarrow 0^+$ and $2_2^+ \rightarrow 2_1^+$ transitions in ^{20}O, detected at three emission angles ($120°$–$140°$, $140°$–$160°$ and $160°$–$180°$), are presented. For the $2_1^+ \rightarrow$ g.s. line, the average difference is 0, since its emission occurs outside the target, while for the $2_2^+ \rightarrow 2_1^+$ line, a deviation from tabulated energy, increasing with increase of the angle, is visible. The same trend is observed for the ^{18}O transition with known lifetime of 27 fs [8, Fig. 4], and other short (below ~ 300 fs) transitions in the O region (for example, for the $7/2^+$ level in ^{19}O with lifetime of 92 fs).
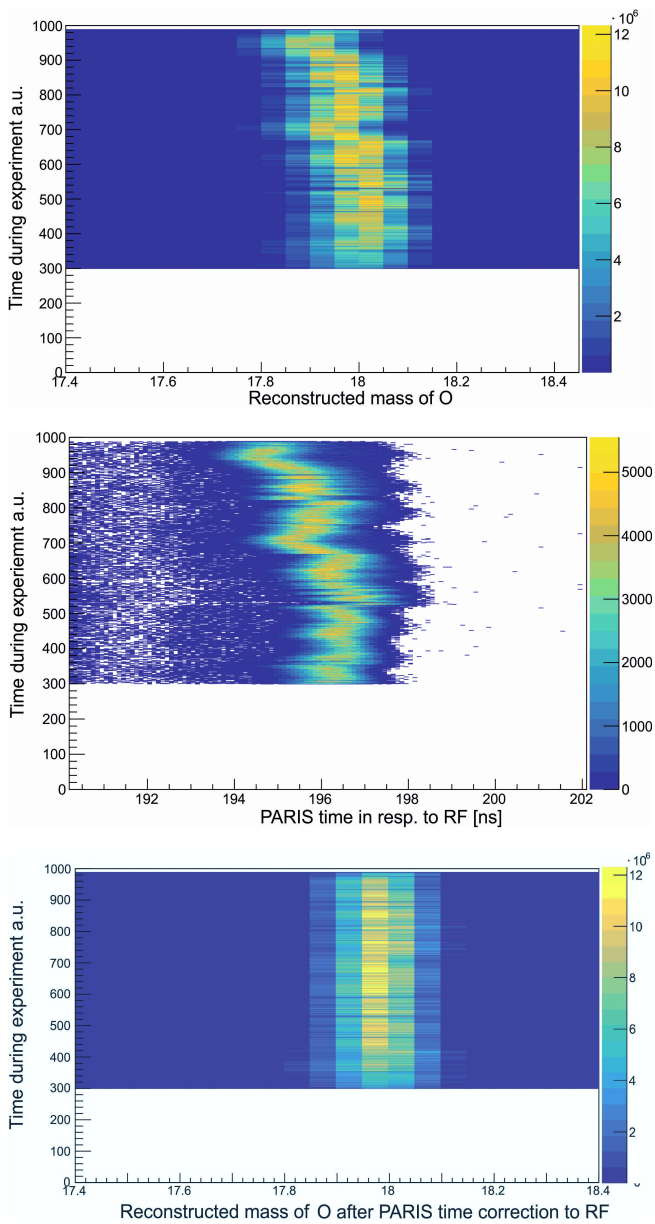
Fig. 5. Upper panel: reconstructed ^{18}O mass drift during the experimental time. Middle panel: PARIS detectors time-signal with respect to the RF, with the same drift pattern. Bottom panel: reconstructed ^{18}O mass with the RF drift corrected by using the PARIS timing information.
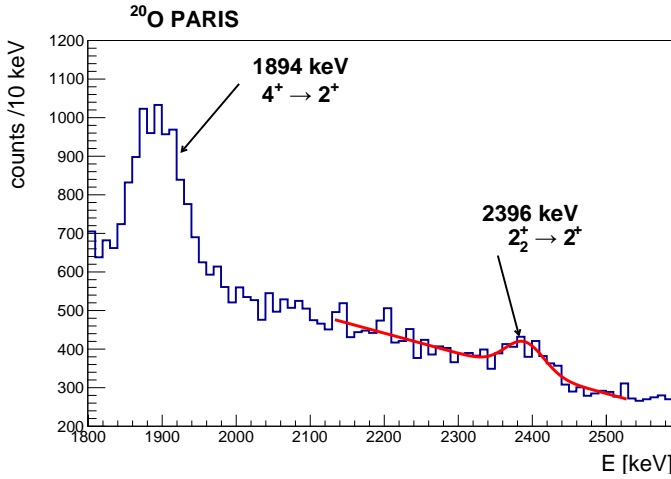
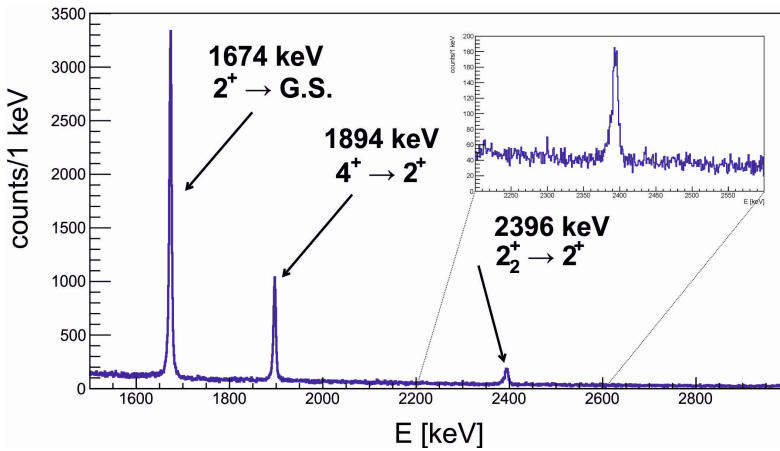Fig. 6. PARIS Doppler-corrected γ-ray spectrum for ^{20}O ions.

Fig. 7. ^{20}O Doppler-corrected γ-ray energy spectrum measured with AGATA (inset – $2_2^+ \rightarrow 2_1^+$ transition).

To extract the value of the lifetime from the experimental data, simulations with variable lifetime and γ-ray energy are needed. Varying the γ-ray energy is necessary because of the lack of precise determination of its value for the ^{20}O $2_2^+ \rightarrow 2_1^+$ transition in literature [9, 10].

The simulation process is divided into five stages:

— Event generator:
  The beam is passing through the target decreasing its energy.
  Multi-nucleon transfer is taking place with linear probability in the target.

After the reaction, the kinetic energy of the fragments is calculated assuming the excitation of both fragments (tuned by experimentally measured ions velocity distribution).

An excited level is let to decay with fixed lifetime τ, emitting γ rays isotropically, with a Doppler shift calculated using the current ion velocity. If the emission occurs inside the target, the ion is processed to the end of target.

γ-ray and ion energies and directions are written to the output file.

— AGATA simulation:

The data produced in the previous step are used as input to the AGATA simulation package [11], which is being configured for the GANIL 31 AGATA crystals detector geometry. As output, the energy deposited in the AGATA crystals, together with the velocity vector of every γ-ray emitter, is written.

— AGATA tracking:

AGATA simulated data are tracked (the same as experimental data) and Doppler corrected. The output is written as: γ-ray energy, detector_ID, relative theta between γ-ray and ion and ion velocity.

— Adding detector response:

Experimentally extracted energy resolutions for the AGATA crystals and differences in counting rates are being included in the simulated data.

— Comparison:

Simulated data are compared to experimentally measured γ-ray spectra calculating χ^2.

4. Conclusions and outlook

Gamma-ray energy shifts of the $2_2^+ \rightarrow 2_1^+$ transition in ^{20}O, displayed as a function of the angle between the γ-ray direction and the ion velocity, showed sensitivity of these shifts to the lifetime of the 2_2^+ excitation (Fig. 8) and indicated that it is below ~ 300 fs. It has also been verified that the statistics collected for the $2_2^+ \rightarrow 2_1^+$ transition in ^{20}O is sufficient to determine the lifetime of the second 2^+ state by using the line-shape technique.

Simulations of the line-shape as a function of lifetime and transition energy have been developed. Finally, two-dimensional (lifetime and γ-ray energy) minimization of χ^2 constructed as comparison of experimental and simulated ^{20}O γ-ray lineshapes will be performed. This will lead to the determination of the lifetime value of the second 2^+ state in ^{20}O.
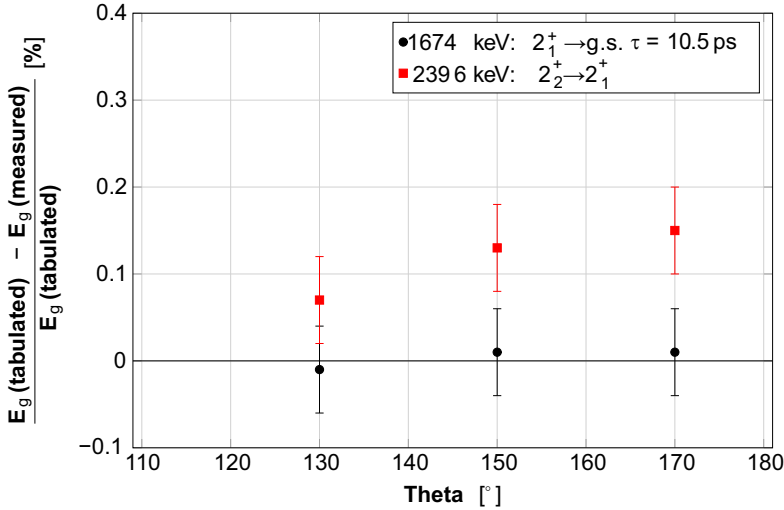
Fig. 8. Relative differences between measured and tabulated energies as a function of the emission angle for $2_1^+ \to$ g.s. and $2_2^+ \to 2_1^+$ ^{20}O γ-rays.

REFERENCES

[1] G. Hagen *et al.*, *Phys. Rev. Lett.* **108**, 242501 (2012).

[2] C. Forssen *et al.*, *J. Phys. G: Nucl. Part. Phys.* **40**, 055105 (2013).

[3] S. Akkoyun *et al.*, *Nucl. Instrum. Methods Phys. Res. A* **668**, 26 (2012).

[4] E. Clèment *et al.*, *Nucl. Instrum. Methods Phys. Res. A* **855**, 1 (2017).

[5] M. Rejmund *et al.*, *Nucl. Instrum. Methods Phys. Res. A* **646**, 184 (2011).

[6] A. Maj *et al.*, *Acta Phys. Pol. B* **40**, 565 (2009).

[7] M. Vandebrouck *et al.*, *Nucl. Instrum. Methods Phys. Res. A* **812**, 112 (2016).

[8] S. Ziliani *et al.*, *Acta Phys. Pol. B* **50**, 625 (2019), this issue.

[9] M. Wiedeking *et al.*, *Phys. Rev. Lett.* **94**, 132501 (2005).

[10] M. Stanoiu *et al.*, *Phys. Rev. C* **69**, 034312 (2004).

[11] M. Labiche *et al.*, AGATA Geant4 Simulations for AGATA@GANIL.